

STELLAR POPULATIONS IN THE OUTER HALO OF THE MASSIVE ELLIPTICAL M49

J. CHRISTOPHER MIHOS,¹ PAUL HARDING,¹ CRAIG S. RUDICK,² AND JOHN J. FELDMEIER³

Draft version April 3, 2024

ABSTRACT

We use deep surface photometry of the giant elliptical M49 (NGC 4472), obtained as part of our survey for diffuse light in the Virgo Cluster, to study the stellar populations in its outer halo. Our data trace M49’s stellar halo out to ~ 100 kpc ($7r_e$), where we find that the shallow color gradient seen in the inner regions becomes dramatically steeper. The outer regions of the galaxy are quite blue ($B-V \sim 0.7$); if this is purely a metallicity effect, it argues for extremely metal poor stellar populations with $[\text{Fe}/\text{H}] < -1$. We also find that the extended accretion shells around M49 are distinctly redder than the galaxy’s surrounding halo, suggesting that we are likely witnessing the buildup of both the stellar mass and metallicity in M49’s outer halo due to late time accretion. While such growth of galaxy halos is predicted by models of hierarchical accretion, this growth is thought to be driven by more massive accretion events which have correspondingly higher mean metallicity than inferred for M49’s halo. Thus the extremely metal-poor nature of M49’s extended halo provides some tension against current models for elliptical galaxy formation.

Subject headings: Galaxies: elliptical and lenticular, cD — Galaxies: evolution — Galaxies: halos — Galaxies: individual (M49) — Galaxies: stellar content

1. INTRODUCTION

Mounting evidence suggests that elliptical galaxies grow through a two-phase process. The rapid assembly of gas-rich clumps at high redshift likely results in a highly dissipative collapse process not too dissimilar to “monolithic collapse” models for elliptical galaxy formation. This leads to the formation of dense, compact spheroidal galaxies (Khochfar & Silk 2006), similar to objects seen in recent high redshift galaxy surveys (e.g., Zirm et al. 2007; van Dokkum et al. 2008). These systems are significantly more compact than local ellipticals, and need to grow in size to become the ellipticals we see today. This argues for a second assembly phase involving later accretion of low mass objects with higher specific angular momentum in order to build up the outer envelopes of the growing ellipticals (e.g., Naab et al. 2007; Oser et al. 2012).

Under this hierarchical model, the outskirts of nearby elliptical galaxies should harbor a variety of signatures of this formation process. Dissipative collapse should lead to strong metallicity gradients (Carlberg 1984; Arimoto & Yoshii 1987), but mergers effectively mix the inner galaxy and largely wash out the gradients (White 1980; Mihos & Hernquist 1994). However, since this mixing is not perfect, the outer halos should still retain a truly metal-poor population of stars. Subsequent accretion of low mass galaxies would then deposit stars with a broad range of metallicities into the outer halo, building up the halo’s surface brightness and mean metallicity. Unlike the rapid mixing in the inner regions, the low density and larger dynamical timescales in galaxy outskirts

mean that the morphological signatures of accretion – shells and streams of stars – survive longer at large radius. Indeed, a variety of deep imaging studies show that many ellipticals have extended tidal debris from late accretion events (e.g., Malin & Carter 1983, Tal et al. 2009, Janowiecki et al. 2010).

While the structure of elliptical galaxy halos can be probed by deep imaging, their extremely faint surface brightness makes detailed studies of their stellar populations difficult. For sufficiently nearby ellipticals, the discrete stellar populations can be imaged using the *Hubble Space Telescope* (HST), giving strong constraints on the age and metallicity of the stars (e.g., Rejkuba et al. 2005, 2011; Harris et al. 2007). Stellar populations in more distant ellipticals must be studied using their integrated colors or spectra. These studies generally show that ellipticals have a gradual radial decline in the mean metallicity over the inner few effective radii (r_e), with gradients of $d[\text{Fe}/\text{H}]/d\log(r) \sim -0.1$ to -0.3 (e.g., Peletier et al. 1990, Kobayashi & Arimoto 1999). However, most studies generally do not probe the outer halo, where the stellar populations may have quite sub-solar metallicities. Moreover, as the most massive ellipticals tend to live near the center of galaxy clusters, studies of their outer halos are complicated by contamination from the more extended intracluster starlight (ICL) surrounding them. As such, the chemical abundance constraints contained in the outer halos of giant ellipticals have remained largely untapped. In this Letter, we present deep imaging of the massive elliptical M49 ($\log M_* = 11.9$, Côté et al. 2003), which lives in the outskirts of the Virgo cluster where ICL contamination is minimized, to study the stellar populations in its outer halo.⁴

2. OBSERVATIONS

mihos@case.edu, paul.harding@case.edu,
 craig.rudick@phys.ethz.ch, jfeldmeier@ysu.edu

¹ Department of Astronomy, Case Western Reserve University, 10900 Euclid Ave, Cleveland, OH 44106

² Institute for Astronomy, ETH Zurich, CH-8093, Zurich, Switzerland

³ Department of Physics and Astronomy, Youngstown State University, Youngstown, OH 44555, USA

⁴ In this paper we adopt a distance of 16 Mpc (Mei et al. 2007) and effective radius of $194''$ (Kormendy et al. 2009) for M49.

We observed M49 as part of our deep imaging survey of diffuse light in the Virgo Cluster using Case Western Reserve University’s 24/36” Burrell Schmidt telescope. We give a brief description of the dataset here; more details can be found in our earlier papers (Mihos et al. 2005; Janowiecki et al. 2010; Rudick et al. 2010). Fields around M49 were imaged in Spring 2006 and 2007 in Washington M, and again in Spring 2011 in a custom B filter; these filters are similar to standard Johnson B and V, but $\sim 300\text{\AA}$ bluer. Each dataset consists of a large number of overlapping images with individual exposure times of 1200s in B and 900s in M, yielding sky levels of ~ 800 and 1300 ADU respectively. The images were flatfielded using a night sky flat constructed from 50–100 offset blank sky pointings. After subtracting the extended wings of bright stars and masking discrete sources on each image (stars, background galaxies, and the bright inner regions of large galaxies), sky subtraction was achieved by subtracting planes fit to the unmasked background sky.

The photometric transformation to Johnson B and V magnitudes was derived using Landolt UBVRI standards to measure the filter color terms, and the ~ 200 stars on each frame with accurate SDSS photometry to derive the photometric zeropoints (employing the Lupton 2005 *ugriz* to Johnson transformation). The solutions showed a residual scatter of 0.02–0.03 mag in the photometry of individual stars and 0.01 mag scatter in the frame-to-frame zeropoints. The individual images were then scaled to a common zeropoint and median combined into final B and V mosaics. In these mosaics, there are typically 30–50 and 40–90 images contributing to any given pixel in the B and V mosaics, respectively.

At low surface brightness, accurate background subtraction and noise estimation is critical to measurements of surface brightness and color. To estimate and correct for uncertainty in the residual background around M49 we identify 50 circular background apertures, $1.5'$ in radius, located 30–60' from M49’s center (beyond the area shown in Figure 1). In these regions, the average residual background is $+0.4$ ADU in B and -1.0 ADU in V, with 1σ per-pixel noise of 0.75 and 1.0 ADU in B and V, respectively. This gives us 2.5σ limiting surface brightness of $\mu_{B,\text{lim}} = 28.7$ and $\mu_{V,\text{lim}} = 28.3$, and we correct the photometric data for Galactic extinction using values of $A_V = 0.061$ and $A_B = 0.081$ (Schlafly & Finkbeiner 2011).

Finally, to increase signal-to-noise at low surface brightness the B and V mosaics were masked and spatially rebinned to $13''$ resolution. In this process, discrete objects on the mosaic were again masked, after which the mosaics were rebinned into 9×9 pixel ($13''\times 13''$) bins, calculating the median intensity of the unmasked pixels in each bin. In the analysis that follows, the full resolution mosaic are used to measure the photometric properties of M49’s inner high surface brightness regions, while the rebinned mosaics are used at larger radius and lower surface brightness.

3. RESULTS

Figure 1 shows our V image of M49 (top) along with a residual image (middle) adapted from Janowiecki et al. (2010), constructed by subtracting an elliptical model of M49’s light profile. A number of accretion shells and streams can be seen surrounding M49; these are dis-

cussed in more detail in Janowiecki et al. (2010) and have been subsequently confirmed by Arrigoni Battaia et al. (2012). The bottom panel of Figure 1 shows our new B–V colormap of M49, binned to $13''\times 13''$ resolution. In this image, we have “unmasked” the high surface brightness regions of the galaxies to give visual continuity to the image and show color across all surface brightnesses.

M49’s color gradient can be clearly seen in the image, with colors ranging from $B-V \sim 1$ at $15''$ to $B-V < 0.7$ in the outskirts ($r > 1000''$). Projected on the face of M49 are two blue star-forming companions, VCC1249 $5'$ to the southeast and NGC 4470 $10'$ to the south. To the northwest of M49, the extended debris shell seen in the residual map can also be seen in the colormap; the shell region is redder than the rest of M49’s halo at similar radius ($r_{\text{sm}} = 20'$ or 90 kpc). In contrast, the shells to the southeast do not show any noticeable features in the colormap. This is not surprising as these shells are at smaller radius ($r_{\text{sm}} = 12.5'$ or 60 kpc), where M49’s halo is both brighter and redder. The southeastern shells contribute less light to the color signal here and, if they are similar in color to the northwest shells, would be similar in color to M49’s halo at that radius.

To extract the quantitative color profile of M49, we first mask M49’s companion galaxies out to their $\mu_V \sim 28.5$ mag arcsec $^{-2}$ isophote as measured in the residual image in Figure 1. We then calculate the median surface brightness and color of all unmasked pixels in elliptical annuli of constant ellipticity $\epsilon = 0.28$ and position angle $\text{PA} = -31^\circ$ (Kormendy et al. 2009; Janowiecki et al. 2010). Measured this way, the derived surface brightness and color are areal-weighted rather than luminosity-weighted, and should be more indicative of the diffuse halo, unbiased by contamination from any discrete unmasked objects that fall within the annuli. The quartile errorbars on the outer points reflect the effects of background subtraction uncertainty, and are calculated by bootstrap sampling the background apertures and recalculating the profiles for each background estimate.

M49’s color profile (Figure 2) shows a very shallow gradient in the inner regions which becomes much steeper at large radius. Inside of $r=100''$ (8 kpc), the logarithmic color gradient is $\Delta(B-V) \equiv d(B-V)/d\log r = -0.03$ mag dex $^{-1}$, but the gradient steepens continuously with radius, reaching values of -0.3 mag dex $^{-1}$ out at $r=800''$ (64 kpc). At the outermost point we measure, the color has dropped to an extremely blue $B-V=0.66\pm 0.02$.

Inside an effective radius, our photometry compares well to previously published data for M49, all of which show a systematic bluing of the colors with increasing radius. Our B–V colors and gradient match those measured by Idiart et al. (2003), and, assuming old stellar populations, are commensurate with gradients measured in other optical colors (Bender & Mollenhoff 1987, Peletier et al. 1990, Kim et al. 2000). At larger radius, however, the situation becomes more complicated. Cohen (1986) measure continual bluing in $g-i$ out to $\sim 350''$, but a reddening in $g-r$, while Kim et al. (2000) show a gradual reddening from $200''$ – $500''$ in C–T $_1$. At these radii, M49’s surface brightness is well below sky, making the derived color gradients very sensitive to accurate sky subtraction. In our data, however, the rapid change in slope becomes clearly noticeable at 30 kpc

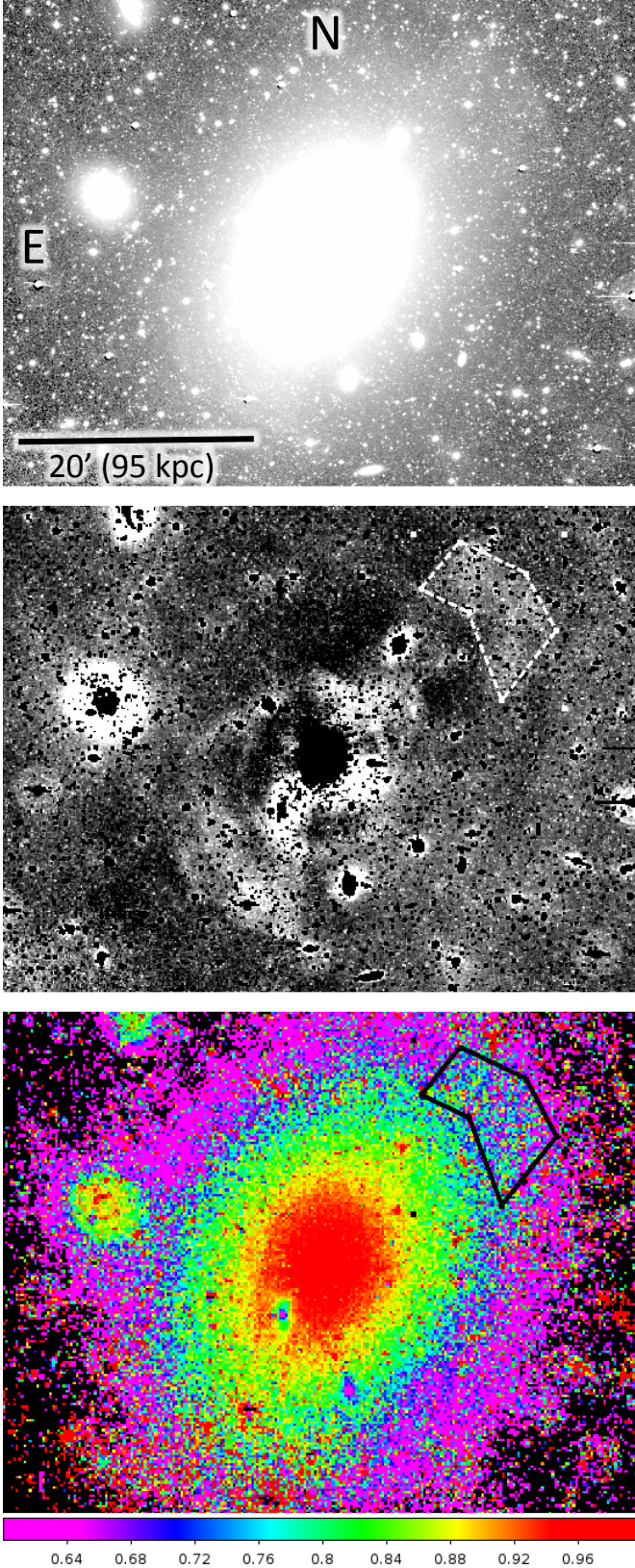


Figure 1. Top: V band image of M49. Center: Binned residual image after isophotal subtraction (from Janowiecki et al. 2010) showing the tidal debris. Bottom: B–V color map, binned to $13''$ resolution. The NW Shell is marked.

($2r_e$), where the sky uncertainty is only $\sim 1\%$ of the measured surface brightness. Even in our outermost radial bin, the surface brightness is a magnitude above the per-pixel sky noise, and the errorbars on those points reflect the effects of the global sky uncertainty. Clearly, errors in sky subtraction are not the cause of the rapid bluing we see at large radius in M49.

4. DISCUSSION

Color trends in elliptical galaxies – both radial gradients within galaxies and trends between color and luminosity in galaxy populations – are well-established to be driven largely by metallicity effects. Figure 3 shows the relationship between B–V color and metallicity for single stellar population (SSP) models from Bruzual & Charlot (2003), using a Chabrier IMF and Padova isochrones. For $[\text{Fe}/\text{H}] > -1$ and populations older than a few Gyr, our inner color gradient translates to a metallicity gradient of $\Delta[\text{Fe}/\text{H}] = -0.15 \text{ dex dex}^{-1}$, similar to the metallicity gradient derived by Peletier et al. (1990) using B–R colors, but somewhat more shallow than those derived spectroscopically, which suggest metallicity gradients of -0.2 to $-0.3 \text{ dex dex}^{-1}$ (Kobayashi & Arimoto 1999). The gradient steepens in the outskirts; if interpreted solely as a metallicity effect, by the inferred gradient reaches $\Delta[\text{Fe}/\text{H}] = -2$ to -3 dex dex^{-1} by $1000''$. The rapid steepening of the color profile begins at approximately the same radius where the luminosity profile begins to show excess light above a pure $r^{1/4}$ law, perhaps suggesting that instead of a simple steepening of the metallicity gradient, we may be seeing a more discrete transition from a metal-rich component to a metal-poor component (e.g., Harris et al. 2007). For old populations, metallicities in the range $[\text{Fe}/\text{H}] = -1$ to -1.5 are needed to explain the extremely blue colors of the outer isophotes, metallicities similar to those of M49’s metal-poor globular cluster system ($[\text{Fe}/\text{H}] \sim -1.3$; Geisler et al. 1996, Cohen et al. 2003).

In principle, the steep gradient could also be explained by systematically younger population ages at large radius. If we extrapolate the shallow inner metallicity gradient outwards, we would expect metallicities in the outer halo of $[\text{Fe}/\text{H}] \sim -0.15$ to -0.3 . At these metallicities, the only way to match the outer isophotal colors is using stellar populations with SSP-equivalent ages of ~ 2 Gyr (Figure 3). This is unrealistically small; while the recent accretion of a late-type galaxy would lead to younger inferred ages, it would have to be an extremely massive and recent event to so dramatically affect the luminosity-weighted age. Given that the accretion features we see in M49 amount to only $\sim 1\%$ of the galaxy’s luminosity (Janowiecki et al. 2010) and are morphologically akin to those expected from a minor merger (Hernquist & Quinn 1989), such a scenario is unlikely. Adopting a moderately lower halo metallicity of $[\text{Fe}/\text{H}] \sim -0.7$, raises the inferred population ages to ~ 3 – 6 Gyr, still quite young for a SSP-equivalent luminosity-weighted age. Halo metallicities of $[\text{Fe}/\text{H}] \leq -1$ are thus the most likely explanation for the blue colors of M49’s outer halo.

How do these stellar population constraints compare to those in the outskirts of ellipticals more generally? A systematic comparison is difficult, as few studies have probed elliptical halos beyond a few r_e . What information does exist shows a wide range of properties: in

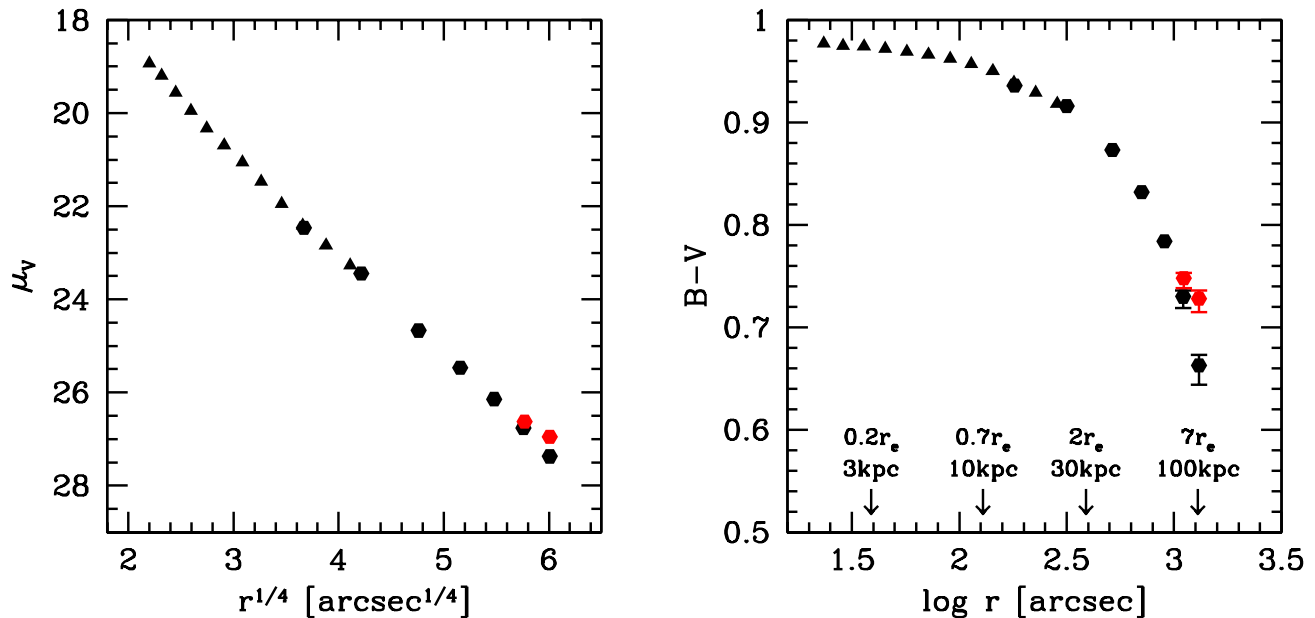


Figure 2. Left: Surface brightness profile of M49. Right: Color profile. Black points represent azimuthally-average profiles; triangles are measurements made from the mosaic at native $1.45''$ resolution, while hexagons show the profiles computed after re-binning to $13''$ resolution. Errorbars represent the effect of background uncertainty on the profiles, and are only larger than the point size in the outermost points in the color profile. In both panels, red points denote measurements made along an angular wedge containing the NW Shell.

some systems the inner metallicity gradients continue smoothly out to $2\text{--}4\ r_e$ (Weijmans et al. 2009; Greene et al. 2012), while others show gradients which either steepen or flatten at large radius (Baes et al. 2007; Foster et al. 2009). Inferred halo metallicities span the range $-1.5 < [\text{Fe}/\text{H}] < 0$ (Baes et al. 2007, Foster et al. 2009, Greene et al. 2012). While most age estimates tend to yield older ages in the outer halo (8-12 Gyr; Baes et al. 2007; Greene et al. 2012). In cases where younger ages are inferred, there is evidence for a recent accretion event in the galaxy’s halo (e.g., NGC 3348; Baes et al. 2007). While our data suggest that M49’s outskirts are at the extreme end of the inferred age/metallicity ranges in these other studies, we stress the very large radii being probed; restricting our analysis to the inner few r_e would show only a modest population gradient similar to those previously determined.

For a few nearby ellipticals, additional information comes from HST studies of resolved stellar populations in their outer halos. NGC 5128 (Centaurus A) shows a mean metallicity of $[\text{Fe}/\text{H}] = -0.5$ at $r = 40\text{ kpc}$ ($7r_e$, Rejkuba et al. 2005), while NGC 3379 shows an extremely broad metallicity distribution at $r = 33\text{ kpc}$ ($12r_e$) with a mean metallicity of $[\text{Fe}/\text{H}] = -0.7$ (Harris et al. 2007). These metallicities are comparable to what we infer (assuming old stellar populations) for M49 at similar *physical* radius ($r = 30\text{--}40\text{ kpc}$), but higher when compared at similar scaled radius ($r/r_e \sim 10$). NGC 5128 also shows evidence for a second population of younger stars (ages $\sim 2\text{--}4\text{ Gyr}$) in its stellar halo (Rejkuba et al. 2011), likely related to the galaxy’s status as a post accretion system. However, these young stars comprise at most 10% of the mass of the halo, and the inferred integrated $B\text{--}V$ color of NGC 5128 would still be redder than what we observe in the outskirts of M49.

Theoretical expectations for the stellar populations in

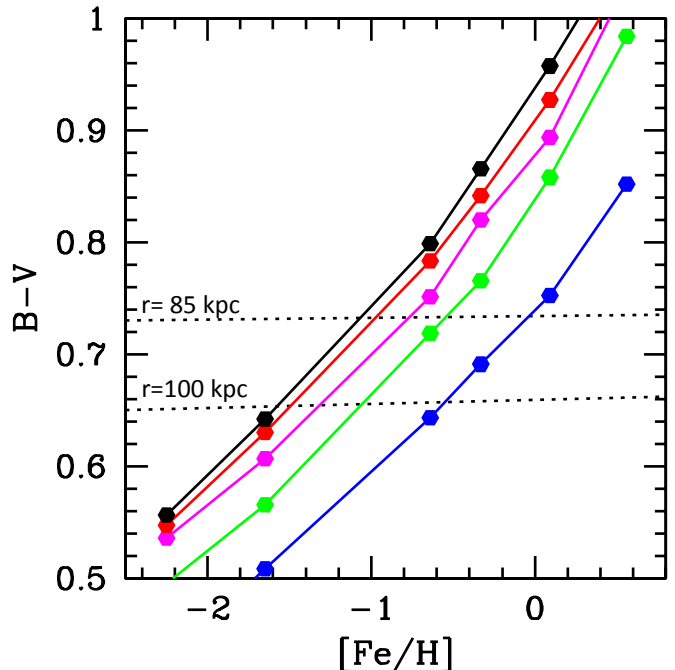


Figure 3. Simple stellar population models from Bruzual & Charlot (2003). From top to bottom, the curves show models with ages 10, 8, 6, 4, and 2 Gyr. The horizontal dashed lines show the color of the two outermost points in our profile.

elliptical halos are similarly diverse. While an initial dissipative collapse should yield strong metallicity gradients (Larson 1974; Carlberg 1984; Arimoto & Yoshii 1987), subsequent merging effectively mixes the inner regions (White 1980; Mihos & Hernquist 1994; Kobayashi

2004), leaving behind the weak gradients observed inside a few r_e . However, chemodynamic simulations of elliptical galaxy formation (Kobayashi 2004) show that the outer metallicity gradients can remain quite steep, yielding metallicities of $[\text{Fe}/\text{H}] < -1$ at large radius. Of course, additional accretion of satellite systems can deposit stars of varying age and metallicity to the outer halo, leading to wider diversity in the halo stellar populations.

Indeed, our photometry directly shows the effect of satellite accretion on the halo populations in M49. The NW Shell is ~ 0.07 mags redder than the surrounding halo; since this region consists of light from both the shell and from M49's (bluer) halo, the intrinsic color of the Shell must be even redder, with $B-V \sim 0.85$. The fact that the shells are redder than the surrounding halo can be understood in terms of a disruptive accretion event. Because of the mass-metallicity relationship, the mean color of the accreted satellite will be bluer than that of M49 as a whole, but can be redder than M49's outer halo. For example, van Zee et al. (2004) show that the population of dE's in Virgo has a mean $B-V$ color of 0.77 at $m_B = 15$ (roughly 1% the luminosity of M49); if a system like these were accreted by M49, it would leave a shell system much like what is shown in Figure 1.

In the picture painted here, M49's metal-poor halo is a relic of the rapid early assembly of the galaxy, while ongoing accretion (as seen in the tidal shells) continues to build the halo mass and metallicity over time. However, this scenario is not without problems. With a velocity dispersion of 280 km s^{-1} and effective radius of 15 kpc, M49 sits squarely on the mass-size relationship for galaxies in the local universe (van der Wel et al. 2008). In other words, M49 has *already* built its halo to modern-day standards, but has done so while retaining its metal-poor nature. Simulations suggest that the dominant mode of halo growth is via minor mergers with typical mass ratios of 1:5 (Oser et al. 2012); such mergers likely would have deposited stars with significantly higher metallicity than that inferred for M49's halo. This tension between a fully-developed halo and its low metallicity remains unresolved.

It is interesting in this context to compare M49 to M87, the giant elliptical at the heart of Virgo. While the two galaxies are comparable in luminosity, M87 has a higher Sersic index ($n = 11.8$, compared to M49's $n = 6.0$; Kormendy et al. 2009) and flatter color gradient (Rudick et al. 2010) at large radius than M49. Where it sits, M87 is also subject to a constant bombardment of satellite galaxies; this dynamically active environment continually adds material to M87's outer halo, as well as the ICL around M87 (Mihos et al. 2005), resulting in the more extended envelope with relatively high mean metallicity. In contrast, M49 lies on the outskirts of the Virgo Cluster, projected 1.2 Mpc from the cluster center, and may be falling into Virgo for the first time (Irwin & Sarazin 1996; Janowiecki et al. 2010). As such, its halo may be more indicative of ellipticals in field and group environments, and be less "processed" than cluster ellipticals.

Stellar populations in the halos of ellipticals hold important information on the processes shaping today's elliptical galaxies. If M49's extended but extremely metal-poor halo is a common feature in massive ellipticals,

a revision of galaxy formation models may be necessary. Progress on these issues requires a better census of the halo stellar populations in ellipticals. Unfortunately, broadband colors are a very blunt tool for constraining stellar populations, unsuited for disentangling age and metallicity effects, while the very low halo surface brightness makes more finely-tuned spectroscopic studies difficult. More promising is the study of discrete stellar populations. At the distance of Virgo, deep HST imaging can reach sufficiently far down the red giant branch to provide constraints on the stellar populations, and has been used to study the metallicity distribution in Virgo's intracluster light (Ferguson et al. 1998; Durrell et al. 2002; Williams et al. 2007). A similar study of the outer halos of M49 and other Virgo ellipticals, as well as ellipticals in the nearby field, would provide a direct test of the extremely metal-poor populations inferred from our deep imaging, and open up a new avenue for the study of elliptical galaxies.

This work has been supported by the NSF through grants AST-0607526 and AST-1108964 to JCM and AST-0807873 to JJF. We thank Heather Morrison, Scott Trager, and Antonio Pipino for many useful discussions.

Facility: CWRU:Schmidt

REFERENCES

- Arimoto, N., & Yoshii, Y. 1987, *A&A*, 173, 23
- Arrigoni Battaia, F., Gavazzi, G., Fumagalli, M., et al. 2012, *A&A*, 543, A112
- Baes, M., Sil'chenko, O. K., Moiseev, A. V., & Manakova, E. A. 2007, *A&A*, 467, 991
- Bender, R., & Moellenhoff, C. 1987, *A&A*, 177, 71
- Bruzual, G., & Charlot, S. 2003, *MNRAS*, 344, 1000
- Côté, P., McLaughlin, D. E., Cohen, J. G., & Blakeslee, J. P. 2003, *ApJ*, 591, 850
- Carlberg, R. G. 1984, *ApJ*, 286, 416
- Cohen, J. G. 1986, *AJ*, 92, 1039
- Cohen, J. G., Blakeslee, J. P., & Côté, P. 2003, *ApJ*, 592, 866
- Durrell, P. R., Ciardullo, R., Feldmeier, J. J., Jacoby, G. H., & Sigurdsson, S. 2002, *ApJ*, 570, 119
- Ferguson, H. C., Tanvir, N. R., & von Hippel, T. 1998, *Nature*, 391, 461
- Foster, C., Proctor, R. N., Forbes, D. A., et al. 2009, *MNRAS*, 400, 2135
- Geisler, D., Lee, M. G., & Kim, E. 1996, *AJ*, 111, 1529
- Greene, J. E., Murphy, J. D., Comerford, J. M., Gebhardt, K., & Adams, J. J. 2012, *ApJ*, 750, 32
- Harris, W. E., Harris, G. L. H., Layden, A. C., & Wehner, E. M. H. 2007, *ApJ*, 666, 903
- Hernquist, L., & Quinn, P. J. 1989, *ApJ*, 342, 1
- Idiart, T. P., Michard, R., & de Freitas Pacheco, J. A. 2003, *A&A*, 398, 949
- Irwin, J. A., & Sarazin, C. L. 1996, *ApJ*, 471, 683
- Janowiecki, S., Mihos, J. C., Harding, P., et al. 2010, *ApJ*, 715, 972
- Khochfar, S., & Silk, J. 2006, *ApJ*, 648, L21
- Kim, E., Lee, M. G., & Geisler, D. 2000, *MNRAS*, 314, 307
- Kobayashi, C. 2004, *MNRAS*, 347, 740
- Kobayashi, C., & Arimoto, N. 1999, *ApJ*, 527, 573
- Kormendy, J., Fisher, D. B., Cornell, M. E., & Bender, R. 2009, *ApJS*, 182, 216
- Larson, R. B. 1974, *MNRAS*, 169, 229
- Lupton, R. B. 2005
<http://www.sdss3.org/dr8/algorithms/sdssUBVRITransform.php>
- Malin, D. F., & Carter, D. 1983, *ApJ*, 274, 534
- Mei, S., Blakeslee, J. P., Côté, P., et al. 2007, *ApJ*, 655, 144
- Mihos, J. C., Harding, P., Feldmeier, J., & Morrison, H. 2005, *ApJ*, 631, L41

- Mihos, J. C., & Hernquist, L. 1994, *ApJ*, 427, 112
- Naab, T., Johansson, P. H., Ostriker, J. P., & Efstathiou, G. 2007, *ApJ*, 658, 710
- Oser, L., Naab, T., Ostriker, J. P., & Johansson, P. H. 2012, *ApJ*, 744, 63
- Peletier, R. F., Davies, R. L., Illingworth, G. D., Davis, L. E., & Cawson, M. 1990, *AJ*, 100, 1091
- Rejkuba, M., Harris, W. E., Greggio, L., & Harris, G. L. H. 2011, *A&A*, 526, A123
- Rejkuba, M., Greggio, L., Harris, W. E., Harris, G. L. H., & Peng, E. W. 2005, *ApJ*, 631, 262
- Rudick, C. S., Mihos, J. C., Harding, P., et al. 2010, *ApJ*, 720, 569
- Schlaflly, E. F., & Finkbeiner, D. P. 2011, *ApJ*, 737, 103
- Tal, T., van Dokkum, P. G., Nelan, J., & Bezanson, R. 2009, *AJ*, 138, 1417
- van der Wel, A., Holden, B. P., Zirm, A. W., et al. 2008, *ApJ*, 688, 48
- van Dokkum, P. G., Franx, M., Kriek, M., et al. 2008, *ApJ*, 677, L5
- van Zee, L., Barton, E. J., & Skillman, E. D. 2004, *AJ*, 128, 2797
- Weijmans, A.-M., Cappellari, M., Bacon, R., et al. 2009, *MNRAS*, 398, 561
- White, S. D. M. 1980, *MNRAS*, 191, 1P
- Williams, B. F., Ciardullo, R., Durrell, P. R., et al. 2007, *ApJ*, 656, 756
- Zirm, A. W., van der Wel, A., Franx, M., et al. 2007, *ApJ*, 656, 66